Gradus Vol 13, No 2 (2026)
ISSN 2064-8014
Article no. 2026.2.ENG.010

# DESIGN OF AN INTEGRATED SPROCKET FOR A FORMULA STUDENT VEHICLE

*Dániel Medgyesi* [1,2, 0000-0002-8581-9124*], *Péter Gerse* [1,2, 0009-0006-5036-3936]

1 Department of Innovative Vehicles and Materials, GAMF Faculty of Engineering and Computer Science, John von Neumann University, Hungary
2 Óbuda University Doctoral School on Materials Sciences and Technologies, Hungary
https://doi.org/10.47833/2026.2.ENG.010

***Keywords:***
Formula Student, sprocket, final-drive ratio, lap-time simulation, finite element analysis

***Article history:***
Received 24 Sept. 2026
Revised 5 Nov. 2026
Accepted 10 Nov. 2026

***Abstract***
*This paper presents an integrated aluminium rear sprocket developed to replace an adapter-based assembly in a Formula Student vehicle. An OptimumLap point-mass model was used to investigate the final-drive ratio, with the mass sweep treated as an internal consistency and sensitivity check. The selected 13-tooth front and 45-tooth rear sprockets give the exact ratio 45/13, approximately 3.46. The 313 kg vehicle configuration yields a simulated acceleration time of 3.66 s. A maximum engine torque of 60 Nm, with unit drivetrain efficiency and load multiplier, produces a prescribed rear-sprocket torque of 1155.38 Nm and an equivalent tangential load of 10.154 kN. This load is distributed over three adjacent tooth flanks without explicit chain contact. The Al7075-T651 material is modelled as isotropic and linearly elastic. The 1 mm mesh yields a maximum von Mises stress of 498.66 MPa and a maximum displacement of 0.3484 mm. The stress change between the 2 mm and 1 mm meshes is 0.065%, and the nominal static yield factor is 1.009. The manufactured component has a mass of 330 g, approximately 67% below the nearly 1 kg reference assembly. Track testing, quantitative wear assessment and fatigue analysis remain subjects for future work.*

## 1. Introduction

In the Formula Student competition series, student teams design, manufacture and validate a complete vehicle system. The development of the powertrain is therefore not merely a matter of structural analysis at component level, but involves the integrated management of mass, rotational inertia, gear ratios, manufacturability and reliability. Early technical bulletins from Formula SAE (Society of Automotive Engineers) also emphasise system integration and verifiable engineering decisions [3] [5].

In the vehicle under examination, the rear sprocket was originally a component manufactured for a motorbike, which was connected to the ribbed coupling of the Drexler LSD (Limited Slip Differential) via a separate adapter and five M10 bolts, as shown in Figure 1. The total mass of the assembly was approximately 1 kg. The adapter did not contribute to the primary function between the chain and the differential, but it did increase the rotating mass and the number of connections. The aim of the development was therefore to integrate the ribbed connection directly into the body of the rear sprocket.

* Corresponding author. Email: medgyesi.daniel@nje.hu



*Figure 1. Detail of the chainwheel assembly with the initial adapter*

The basic design requirements were compatibility with the existing 520 chain, a chain pitch identical to that of the small sprocket, a geometry matching the ribbing of the differential gear, a detachable mounting, and adequate static load capacity. The target mass was set at under 300 g. Tooth wear is considered separately as a subject for quantitative testing, since contact between the aluminium tooth surface and the steel chain presents a tribological challenge. The nature of wear, which depends on load, sliding distance and hardness, is described by the Archard model [1].

## 2. Method

### 2.1. Concept development and requirements specification

The conceptual design was based on two main sets of variables: the method of torque transmission and the lightening of the disc body. The joining methods examined were bolted joints, adhesive bonding and ribbed joints (as shown in Figure 2). The principles of mass reduction included a membrane-like disc, a spoked design and localised material removal. Four composite concepts were evaluated using a weighted decision matrix. The variant incorporating direct ribbed bonding, membrane-like mass reduction, axial securing with a retaining ring and an anodised surface took first place with 46 points. The main requirements defined during the design phase are summarised in Table 1.

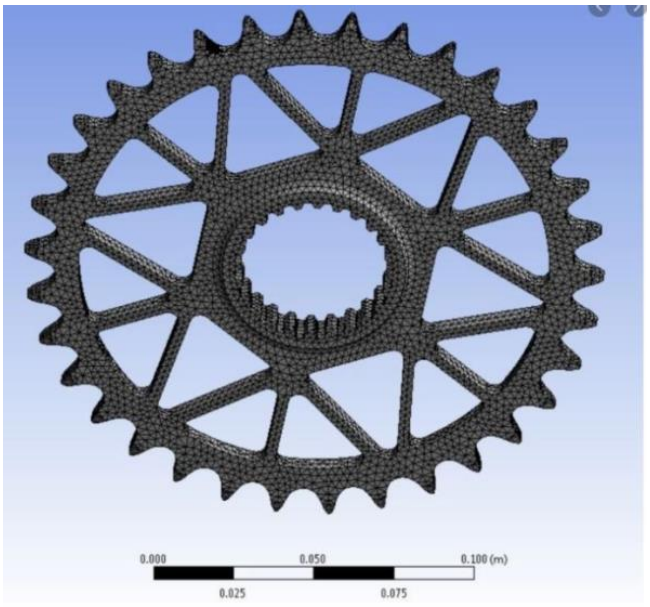


*Figure 2. Integrated ribbed, lightweight sprocket design*

*Table 1. Main requirements for the design*

| Requirement | Target value or condition | Inspection |
|---|---|---|
| Drivetrain compatibility | 520 chain; pitch 15.875 mm, matched sprocket geometry | CAD integration |
| Connection | Direct fit with the Drexler LSD ribbing and detachable axial retention | Assembly test |
| Structural compliance | Maximum von Mises stress not exceeding the adopted 503 MPa yield strength in the specified static load case | Finite element stress comparison |
| Mass | Below 300 g | Weighing |

### 2.2. Determining the final drive ratio

The final-drive ratio was determined using OptimumLap lap-time simulation. OptimumLap uses a quasi-steady-state point-mass vehicle model [11]. The vehicle follows a prescribed track path, and the attainable speed depends on propulsion, braking and tyre-force capacity. Suspension motion, individual-wheel load transfer and transient vehicle responses are not resolved. In the present configuration, constant longitudinal and lateral friction coefficients define a linear dependence of the limiting tyre forces on normal load, as expressed in Eq. (1). This assumption describes force capacity rather than a measured nonlinear force-slip characteristic.

$$F_{x,\lim} = \mu_x N, \qquad F_{y,\lim} = \mu_y N \tag{1}$$

The vehicle-model input parameters are presented in Table 2, and the complete engine torque-speed input is given in Table 3. The tyre radius is expressed in metres. Thermal efficiency and fuel energy density are vehicle-model inputs and are separate from the mechanical drivetrain efficiency used in the structural-load calculation.

*Table 2. Vehicle-model input parameters*

| Parameter | Value | Unit |
|---|---|---|
| Total vehicle mass | 313 | kg |
| Drive type | 2WD (two driven wheels) | - |
| Drag coefficient | 0.9 | - |
| Downforce coefficient | 1.9 | - |
| Frontal area | 1.005 | m² |
| Air density | 1.204 | kg/m³ |
| Tyre radius | 0.235 | m |
| Rolling-resistance coefficient | 0.015 | - |
| Longitudinal friction coefficient | 2.85 | - |
| Lateral friction coefficient | 2.75 | - |
| Engine torque-speed curve | Table 3 | Nm, rpm |
| Thermal efficiency | 0.35 | - |
| Fuel energy density | 47 200 000 | J/kg |
| Transmission type | Sequential gearbox | - |
| Gear ratios 1 to 5 | 2.846, 1.950, 1.556, 1.333, 1.190 | - |
| Final-drive field in the parameter record | 5.862 | - |
| Physical chain final-drive ratio | 45/13 = 3.46 | - |

*A total vehicle mass of 313 kg was used in all vehicle-dynamics simulations except the mass-sensitivity sweep.*

*Table 3. Complete engine torque-speed input*

| Engine speed (rpm) | Torque (N·m) | Engine speed (rpm) | Torque (N·m) |
|---|---|---|---|
| 3000 | 20 | 8000 | 59 |
| 4000 | 53 | 9000 | 58 |
| 5000 | 53 | 10000 | 59 |
| 6000 | 56 | 11000 | 57 |
| 7000 | 60 | 12000 | 55 |

In the base vehicle model, the final-drive ratio was varied at a total vehicle mass of 313 kg. In the mass-sensitivity sweep, the total mass was varied from 260 kg to 320 kg. The remaining input parameters were held fixed within each sweep. Simulations were performed on the FSAE Endurance Germany 2012 and FSAE Acceleration layouts, with track time given primary weighting in the selection. The physical chain ratio is defined by the tooth counts in Eq. (2); the separate reduction field of 5.862 in the vehicle input record has an unspecified definition.

The mass sweep is treated as an internal consistency and sensitivity check. A monotonic, approximately linear response is physically plausible under a one-parameter change, but does not establish predictive accuracy or agreement with the actual vehicle. No validation against measured acceleration, sector times or lap times is claimed. The final-drive study included a broad sweep and a refined comparison over approximately 3.08-3.46, the discrete alternatives and acceleration results are reported in Table 6.

The selected sprocket pair comprises 13 front teeth and 45 rear teeth. Equation (2) defines the exact final-drive ratio.

$$i_{\mathrm{FD}} = \frac{z_{\mathrm{rear}}}{z_{\mathrm{front}}} = \frac{45}{13} = 3.46 \tag{2}$$

Engine-speed use is bounded here by the supplied torque curve, which reaches 60 Nm at 7000 rpm and extends to 12000 rpm. With the highest configured gear ratio of 1.190 and the 0.235 m tyre radius, Eq. (3) gives a kinematic gearing limit of approximately 132.0 km/h at 12000 rpm. The primary ratio is taken from the Yamaha service manual [12]. This value is conditional on the five-gear configuration in Table 2 and does not represent a measured or simulated maximum vehicle speed.

$$v_{\mathrm{kin}} = \frac{2\pi r_w n_e}{60\, i_p i_g i_{\mathrm{FD}}} = 36.68\ \mathrm{m/s} = 132.0\ \mathrm{km/h} \tag{3}$$

The entire development process is summarised in Figure 3.

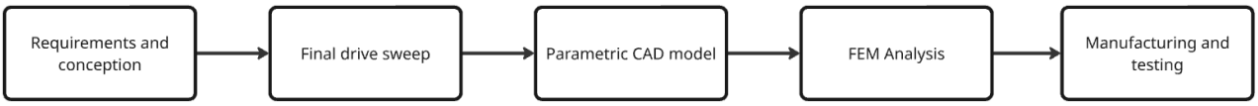


*Figure 3. The main steps in the design and analysis process*

### 2.3. Maximum transmitted torque and equivalent tooth load

The structural load case is derived from maximum engine torque. The calculation assumes that the 60 N·m peak torque is fully transmitted in first gear through the production 2004 Yamaha YZF-R6 drivetrain. The manufacturer service manual gives a primary reduction of 86/44 and a first-gear ratio of 37/13 [12]. Together with the selected 45/13 chain ratio, these values give the total reduction in Eq. (4). The numerical inputs and assumptions are summarised in Table 4.

$$i_{\mathrm{tot}} = i_p i_1 i_{\mathrm{FD}} = \frac{86}{44}\,\frac{37}{13}\,\frac{45}{13} = 19.26 \tag{4}$$

Mechanical drivetrain efficiency is set to η = 1, so transmission losses do not reduce the imposed torque. The additional load multiplier is K = 1, as adopted for the simplified case. Equation

(5) therefore defines a maximum transmitted static torque, without impact or gearshift amplification. It is not an upper bound on all transient drivetrain loads.

$$M_{\mathrm{rear}} = M_e i_{\mathrm{tot}} \eta K = 60 \cdot 19.26 \cdot 1 \cdot 1 = 1155.38 \ \mathrm{Nm} \tag{5}$$

*Table 4. Inputs to the prescribed structural-load calculation*

| Quantity | Value | Source or assumption |
|---|---|---|
| Maximum engine torque | 60 Nm | Table 3; peak at 7000 rpm |
| Primary reduction | 86/44 = 1.9545 | Yamaha service manual [12] |
| First-gear ratio | 37/13 = 2.8462 | Yamaha service manual [12] |
| Chain final-drive ratio | 45/13 = 3.46 | Selected sprocket tooth counts |
| Mechanical efficiency η | 1.0 | Lossless torque-transmission assumption |
| Load multiplier K | 1.0 | Prescribed static case |
| 520 chain pitch | 15.875 mm | Manufacturer chain dimensions [13] |

For a roller chain of pitch p on a sprocket with z teeth, the pitch-circle radius follows from the regular pitch-polygon geometry. The 520 chain pitch is 15.875 mm [13]. For the 45-tooth rear sprocket, Eq. (6) gives the moment arm used to obtain the equivalent tangential load in Eq. (7).

$$r_p = \frac{p}{2\sin(\pi/z)} = \frac{0.015875}{2\sin(\pi/45)} = 0.113789 \ \mathrm{m} \tag{6}$$

$$F_{t,\mathrm{eq}} = \frac{M_{\mathrm{rear}}}{r_p} = \frac{1155.38}{0.113789} = 10\,153.72 \ \mathrm{N} \tag{7}$$

The quantity in Eq. (7) is an equivalent tangential load for the prescribed rear-sprocket torque. It is not a separately determined tight-side chain tension. The simplified model omits chain pretension, slack-side tension and their radial loading effects. Studies of roller-chain load distribution show that elastic deformation and chain tension affect the forces carried by individual sprocket teeth [14,15]. These findings support non-uniform load sharing, while the specific distribution must be stated as a modelling assumption.

The equivalent load is distributed over three adjacent tooth flanks with shares of 50%, 30% and 20%, as listed in Table 5. These shares define the engineering idealisation adopted for the static analysis, they do not represent a measured roller-contact distribution. Each force is distributed over the loaded flank near the pitch circle, with a local direction tangent to that circle and the same torque-producing sense for all three teeth. The load and support arrangement is shown in Figure 4.

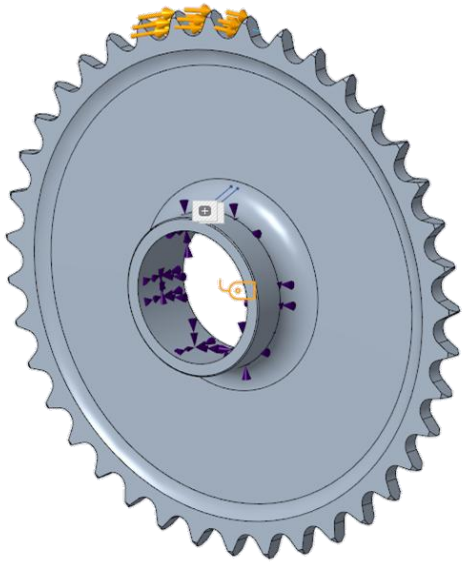

*Figure 4. Static sprocket model with three adjacent tooth-flank loads and constraints at the inner coupling*

*Table 5. Three-tooth representation of the equivalent tangential load*

| Loaded tooth | Share | Force magnitude | Application |
|---|---|---|---|
| First loaded tooth | 50% | 5076.86 N | Distributed over its loaded flank |
| Second adjacent tooth | 30% | 3046.12 N | Distributed over its loaded flank |
| Third adjacent tooth | 20% | 2030.74 N | Distributed over its loaded flank |
| Sum of magnitudes | 100% | 10153.72 N | Nominal pitch-circle representation |

For each distributed surface load, $d_j$ denotes the perpendicular distance between the sprocket axis and the line of action of its resultant. Moment equivalence requires Eq. (8). The nominal values in Table 5 use $d_j = r_p$, their unrounded values reproduce the 1155.38 Nm torque. If the selected surface resultants act at other lever arms, their magnitudes must be adjusted to preserve this moment. The simplification is intended for static structural assessment under the stated boundary load, and does not resolve roller contact pressure or predict local contact stresses [14,15].

$$\sum_{j=1}^{3} F_j \, d_j = M_{\text{rear}} = 1155.38 \text{ Nm} \tag{8}$$

### 2.4. Finite element model

The geometry of the sprocket was created in the Creo Parametric 12 environment. The linear-static structural model consists of the sprocket subjected to the distributed tooth-flank forces in Table 5. The chain is represented by these equivalent surface loads, without explicit chain links or chain-sprocket contact pairs. No contact-friction coefficient is therefore assigned to the chain-sprocket interface. The support symbols in Figure 4 identify the constrained inner coupling region. The aim of the analysis is to investigate the structural response to the prescribed tooth loads. The structured application of the finite element method and the principles of topological material distribution are discussed in the fundamental works [4] [7] [9] [10].

The global settings of the adopted 1 mm mesh are shown in Figure 5. The size-function method is Fixed, with a minimum size of 1 mm, maximum face size of 1 mm and maximum size of 1 mm, the growth-rate parameter is 1.85. Figure 6 shows the discretised sprocket model. Mesh sensitivity was assessed by reducing the nominal element size from 10 mm to 1 mm in 1 mm increments and comparing the maximum von Mises stress across the series. The numerical results and stress trend are presented in Table 8 and Figure 12.

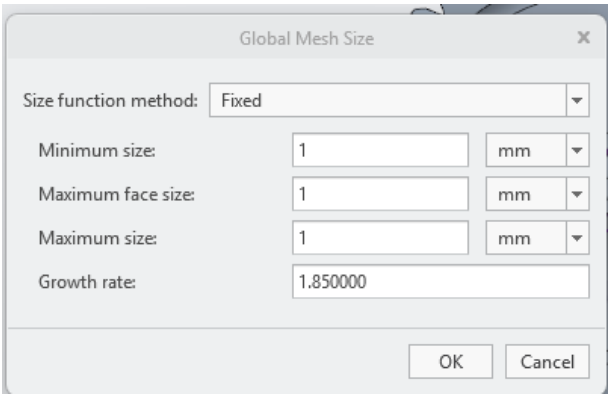


*Figure 5. Final applied global mesh settings with a nominal size of 1 mm*

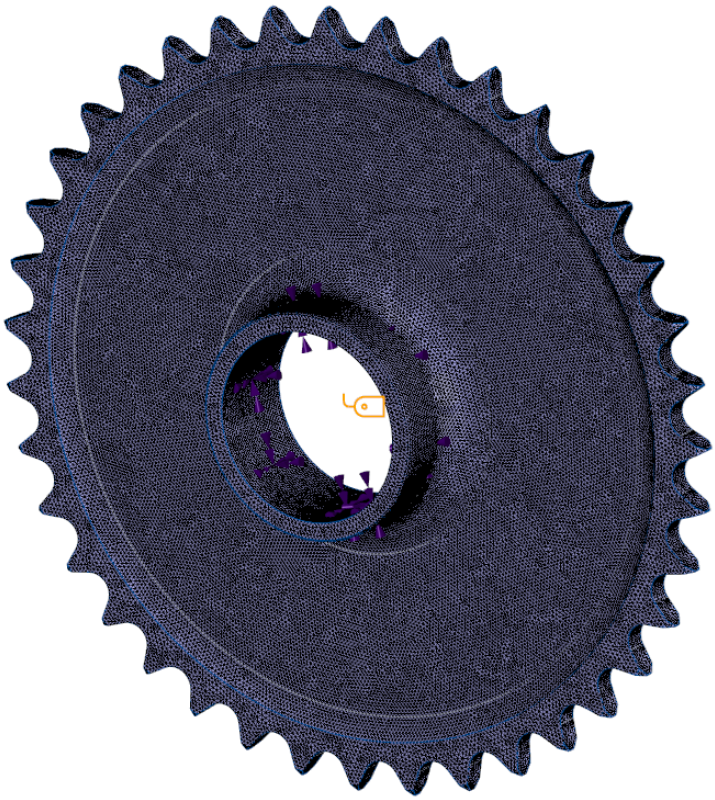

*Figure 6. Final discretised sprocket model and constrained inner coupling region*

The complete material definition entered in the model is reproduced in Figure 7. Al7075-T651 is represented as isotropic and linearly elastic, with Young's modulus E = 71 700 MPa and Poisson's ratio v = 0.30. The density entry is 2.81 × $10^{-9}$ tonne/mm³, equivalent to 2810 kg/m³. The adopted tensile yield stress is 503 MPa and the tensile ultimate stress is 572 MPa. The distortion-energy criterion, identified as von Mises in the material panel, is used for the static yield comparison, no plastic stress-strain law is defined.

The configured coefficient of thermal expansion is zero, and no thermal load is applied in this structural case. Mechanism damping and compressive ultimate stress are left undefined in the material model, and the fatigue model is set to None. The AL7075-T651 designation specifies the assigned alloy condition. Fatigue performance is not evaluated in the present linear-static analysis.

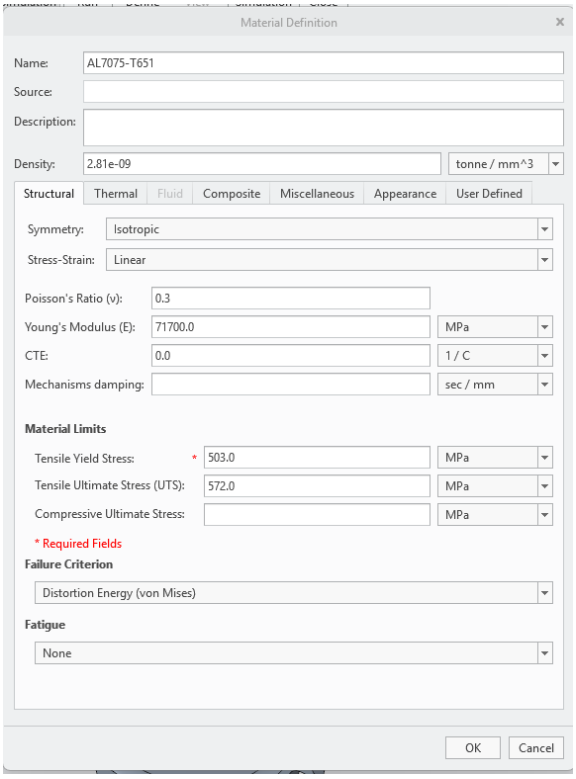


*Figure 7. Complete Al7075-T651 material definition used in the structural model*

# 3. Results

## 3.1. Vehicle dynamics results

The results of the internal consistency and mass-sensitivity check are shown in Figure 8. In the range between 260 and 320 kg, the lap time increased from approximately 84.34 s to 84.76 s. The total change is approximately 0.42 s, which corresponds to an average sensitivity of about 0.007 s/kg. The data points form a regular, nearly linear trend; no inflection points or non-monotonic sections appeared within the range under investigation. This is a numerical sensitivity result and does not validate the model against measured vehicle performance.

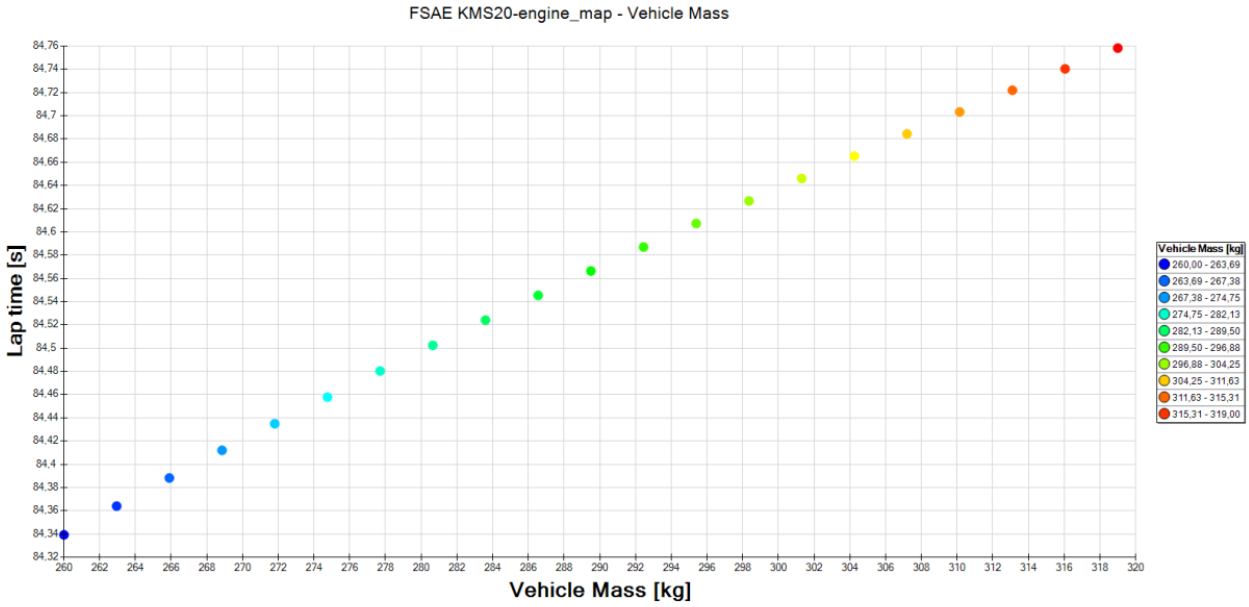


*Figure 8. Internal consistency check showing simulated lap time as a function of total vehicle mass*

The results of the final-drive-ratio sweep are shown in Figure 9. The lap time calculated at a ratio of 2.50 was approximately 87.4 s. As the ratio was increased, the lap time decreased towards the 3.3-3.5 range, after which a plateau of around 84.5-84.6 s was reached. The selected 45/13 ratio falls in this plateau, where the benefit from a further increase in ratio is limited.

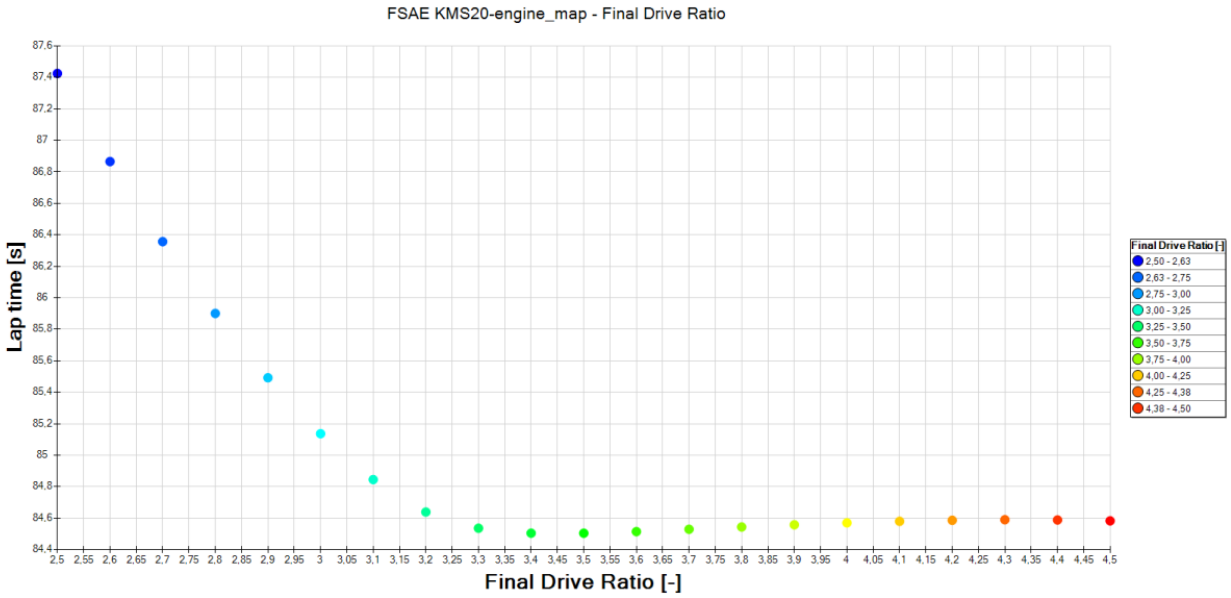


*Figure 9. Simulated lap time as a function of final-drive ratio*

Table 6 presents the track-time and acceleration results of the refined ratio comparison for the 313 kg vehicle configuration. For a fixed 13-tooth front sprocket, the ratios are expressed as rear/front tooth-count fractions. The reference ratio 3.000 corresponds to 39 rear teeth, while the candidate ratios correspond to 40-45 rear teeth.

*Table 6. Track and acceleration results for the 313 kg configuration*

| Front/rear teeth | Exact ratio, decimal | Track time (s) | Acceleration time (s) |
|---|---|---|---|
| 13/39 (reference) | 39/13, 3.0000 | 85.89 | 3.70 |
| 13/40 | 40/13, 3.0769 | 85.61 | 3.70 |
| 13/41 | 41/13, 3.1538 | 85.35 | 3.69 |
| 13/42 | 42/13, 3.2308 | 85.13 | 3.68 |
| 13/43 | 43/13, 3.3077 | 84.95 | 3.67 |
| 13/44 | 44/13, 3.3846 | 84.81 | 3.66 |
| 13/45 | 45/13, 3.4615 | 84.73 | 3.66 |

Within this refined discrete set, the 45-tooth sprocket gives the lowest recorded track time, 84.73 s, while its 3.66 s acceleration time is unchanged from the 44-tooth case at the precision reported. Relative to the 3.000 reference, the track-time reduction is 1.16 s, approximately 1.35%, and the acceleration-time reduction is 0.04 s, approximately 1.08%. The decision therefore retains 45/13 because it combines the minimum recorded track time with no acceleration-time penalty. These results support a comparative selection for the 313 kg vehicle; absolute performance predictions require experimental validation.

The activation rate of the traction-control model is shown in Figure 10. The indicator was approximately 25% at a ratio of 2.5, then exceeded 70% at ratios around 3.4-3.6. The vehicle was not equipped with an actual TCS system during the test period, therefore, this result does not indicate control performance, but rather frequent reaching of the driven wheels' traction limit. A ratio of 45/13 is favourable in terms of lap time, but may also result in greater demands on handling and accelerator-pedal modulation.

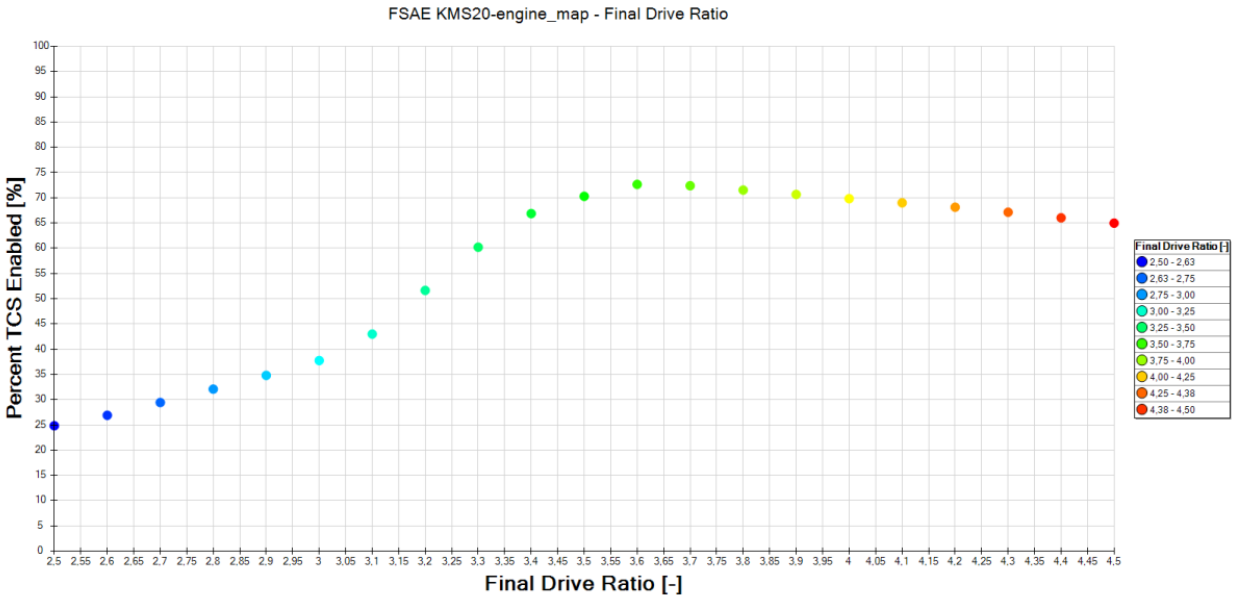


*Figure 10. Activation rate of the TCS model as a function of final-drive ratio*

### 3.2. Finite element analysis

The structural case prescribes a rear-sprocket torque of 1155.38 N·m through three adjacent tooth-flank loads with a nominal total magnitude of 10.154 kN. The mesh and material inputs are documented in Figures 5-7. Figure 11 shows the resulting von Mises stress field. The maximum stress is 498.6587 MPa and the maximum displacement is 0.3484 mm on the 1 mm mesh. The highest displayed stress is located near the loaded tooth flanks in the upper part of the sprocket. The point annotations in Figure 11, 95.1826 MPa and 0.0152707 mm, represent local probe values rather than the global maxima.

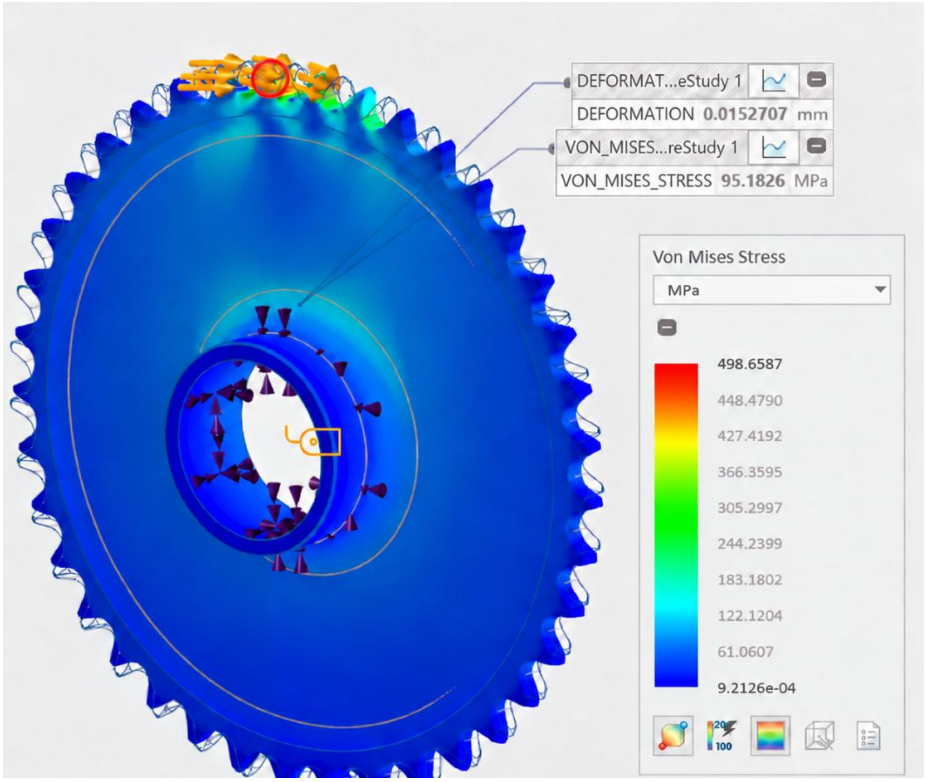


*Figure 11. Von Mises stress field (MPa) for the three-tooth load case, the legend maximum is 498.6587 MPa and the annotations are local probe values*

The three-tooth representation preserves the intended driving moment when the surface resultants satisfy Eq. (8). It is suitable for examining the response to the defined static boundary load, while local tooth-flank stresses depend on the selected loading area and moment arm. Contact pressure, chain dynamics and fatigue life are outside this model. The nominal static yield factor is calculated using the adopted 503 MPa yield strength and the reported global stress maximum, as expressed in Eq. (9).

$$n_y = \frac{\sigma_y}{\sigma_{\mathrm{VM,max}}} = \frac{503}{498.6587} = 1.0087 \approx 1.009 \tag{9}$$

The reported maximum is 4.3413 MPa below the adopted yield strength, satisfying the static stress criterion in Table 1 for this load case. The margin is small, approximately 0.86% of the yield strength. This comparison does not establish a fatigue margin or an allowance for transient load amplification. The main numerical results are summarised in Table 7.

*Table 7. Main numerical results and documented analysis inputs*

| Parameter | Value | Interpretation |
|---|---|---|
| Front/rear sprocket teeth | 13/45 | Exact chain ratio 45/13 |
| Rear-sprocket torque | 1155.38 Nm | 60 Nm in first gear, η = K = 1 |
| Equivalent tangential load | 10 153.72 N | Three adjacent loaded flanks, nominal pitch-circle moment arms |
| Final global mesh size | 1 mm | Settings in Figure 5, mesh in Figure 6 |
| Adopted tensile yield stress | 503 MPa | Linear-elastic material definition in Figure 7 |
| Maximum von Mises stress | 498.6587 MPa | Specified static load case (Figure 11 and Table 8) |
| Maximum displacement | 0.3484 mm | Global maximum from the final mesh run |
| Nominal static yield factor | 1.009 | 503 MPa / 498.6587 MPa (Eq. (9)) |
| Acceleration time | 3.66 s | 313 kg vehicle configuration (Table 6) |
| Final component mass | 330 g | 30 g above the 300 g target |
| Mass reduction | Approximately 67% | Compared with the nearly 1 kg reference assembly |

The mesh-sensitivity results are listed in Table 8. The nominal mesh size was reduced from 10 mm to 1 mm in ten successive runs. For the maximum von Mises stress Q, the relative change between consecutive runs is defined in Eq. (10). The subscripts k and k−1 identify the current, finer mesh and the preceding mesh, respectively; abs denotes the absolute value.

$$\delta_Q^k = \frac{\mathrm{abs}(Q_k - Q_{k-1})}{Q_k}\ 100\% \tag{10}$$

*Table 8. Mesh sensitivity of the maximum von Mises stress*

| Mesh size (mm) | Maximum von Mises stress (MPa) | Stress change (%) |
|---|---|---|
| 10 | 262.4019 | - |
| 9 | 332.7280 | 21.136 |
| 8 | 387.4981 | 14.134 |
| 7 | 428.6567 | 9.602 |
| 6 | 458.1483 | 6.437 |
| 5 | 477.9174 | 4.137 |
| 4 | 489.9084 | 2.448 |
| 3 | 496.0660 | 1.241 |
| 2 | 498.3346 | 0.455 |
| 1 | 498.6587 | 0.065 |

Figure 12 shows the maximum von Mises stress as a function of nominal mesh size, with the numerical results connected by straight line segments. The stress approaches a plateau as the mesh is refined. The change decreases from 0.455% between the 3 mm and 2 mm meshes to 0.065% between the 2 mm and 1 mm meshes. The 1 mm discretisation is retained on the basis of the small change in maximum stress within the investigated refinement range.

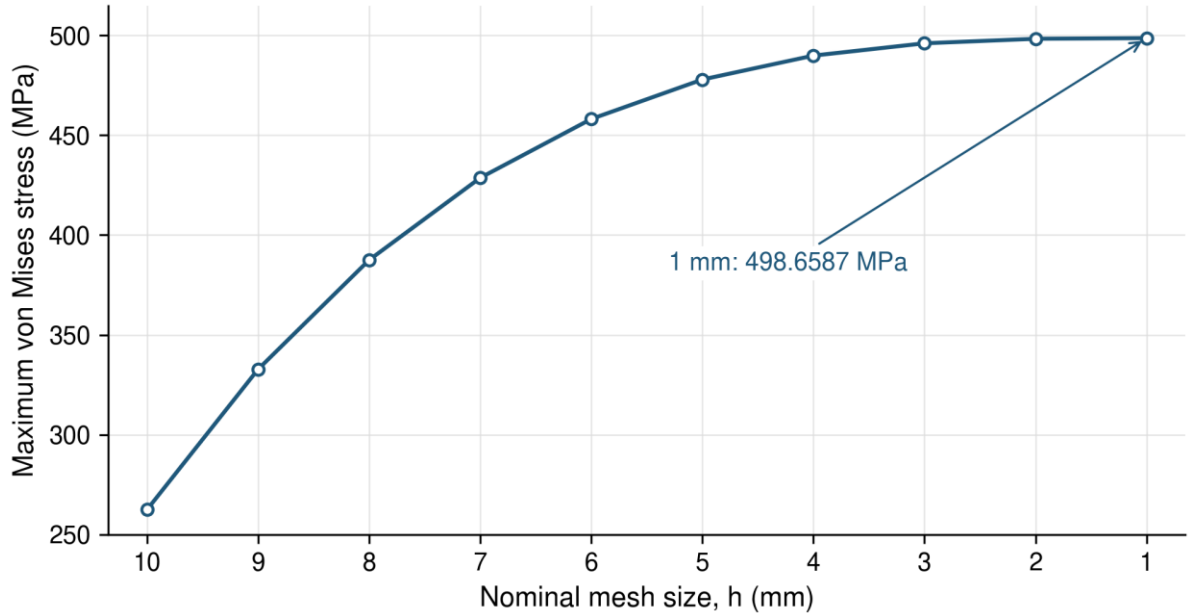


*Figure 12. Maximum von Mises stress versus nominal mesh size for refinement from 10 mm to 1 mm*

The relative changes quantify sensitivity to the sampled mesh sizes rather than error relative to an exact solution. The observed plateau characterises the specified static model and surface loading, it does not quantify the modelling uncertainty associated with the tooth-load distribution or local roller contact.

### 3.3. Manufacture and preliminary testing

Due to the membrane-like thinning of the disc body, it was necessary to use a support device during milling. The outer profile was machined using conventional profile milling, whilst the inner ribbing was produced using wire EDM. Including the procurement of the Al7075-T651 raw material, the production lead time was four days. Due to a measurement discrepancy, the axial dimension of the

first component was 1 mm larger than intended, the fit of the retaining ring was restored by subsequent turning.

The earlier prototype, designed for a gear ratio of around 3, withstood 22 km of continuous track load without structural failure. Visible wear appeared on the teeth. As a result, the tooth thickness was modified, and the use of an anodised surface was considered. The track test of the final 45-tooth version had not yet been carried out at the time of finalizing the documentation, therefore, the conclusions regarding vehicle dynamics and durability are partly based on numerical results.

## 4. Discussion

Based on the final-drive-ratio sweep, the optimum lap time did not appear as a single sharp minimum but as a broad plateau. This allows factors such as handling, wheel slip, engine rev range and component size to be taken into account alongside lap time when selecting the final-drive ratio. The 45/13 ratio is a solution close to the minimum lap time, and the discrete comparison also gives a favourable acceleration time. The high value of the TCS indicator suggests frequent operation at the traction limit. A comparative test on the same track with the same tyre and vehicle settings is required to assess the actual driving behaviour.

The maximum-torque calculation supplies a traceable static boundary load independently of an assumed tyre-grip limit. The three-tooth load split remains an idealisation, and moment equivalence does not establish the accuracy of local contact stresses. Mesh refinement produces decreasing changes in maximum von Mises stress, with a final change of 0.065% at 1 mm. The nominal static yield factor of 1.009 indicates a small margin for the specified load case, and no transient-load or fatigue allowance is established. Except for the mass-sensitivity sweep, all vehicle-dynamics simulations use the 313 kg total mass reported in Table 2. Validation of absolute vehicle performance requires comparison with measured acceleration, sector times or lap times.

Fatigue assessment is reserved for future work and must account for load amplitude, stress ratio, cycle count and surface condition [2] [8]. Crack-growth assessment may subsequently use the Paris-Erdogan relationship [6]. In terms of tooth wear, surface treatment, chain pitch accuracy, chain tension and lubrication conditions are collectively decisive factors. The mass was reduced to 330 g, meaning the original target of 300 g was not met; however, the reduction of approximately 67% compared with the adapter assembly fulfilled the main mass-reduction objective.

## 5. Conclusion

As a result of this development, a spline-coupled rear sprocket made from Al7075-T651 aluminium was produced to replace the adapter-type rear-sprocket assembly. The vehicle-dynamics analysis yielded a lap-time curve that flattened near 3.3-3.5. The selected 13-tooth front and 45-tooth rear sprockets provide the exact final-drive ratio 45/13, approximately 3.4615. For the 313 kg vehicle configuration, the simulated acceleration time is 3.66 s at this ratio. A maximum transmitted static torque of 1155.38 N·m was derived from the 60 Nm engine torque with $\eta = K = 1$, giving a 10.154 kN equivalent tangential load shared by three adjacent tooth flanks. The structural model uses the 1 mm mesh and isotropic, linear-elastic material definition. The maximum von Mises stress is 498.6587 MPa and the maximum displacement is 0.3484 mm. The final mesh-refinement change in maximum stress is 0.065%. The adopted static yield criterion is satisfied with a nominal factor of 1.009. The final component mass is 330 g, approximately 67% below the nearly 1 kg reference assembly. Further work will focus on track testing, quantitative tooth-wear measurement, fatigue assessment and experimental validation of the simulation.

## Acknowledgment

The authors would like to thank KEFO Motorsport, the drivetrain group of the Kecskemét Formula Student team, and Múzsai Metáll Fémipari Kft. for their assistance with manufacturing.

## References


[1] J. F. Archard, "Contact and Rubbing of Flat Surfaces," Journal of Applied Physics, vol. 24, no. 8, pp. 981-988, 1953, doi: 10.1063/1.1721448.

[2] D. Arola and C. L. Williams, "Estimating the fatigue stress concentration factor of machined surfaces," International Journal of Fatigue, vol. 24, no. 9, pp. 923-930, 2002, doi: 10.1016/S0142-1123(01)00145-9.

[3] S. A. Beckel, S. Obregon, and R. D. Matthews, "The 1982 National Intercollegiate Formula SAE Competition," SAE Technical Paper 821093, 1982, doi: 10.4271/821093.

[4] M. P. Bendsøe and N. Kikuchi, "Generating optimal topologies in structural design using a homogenization method," Computer Methods in Applied Mechanics and Engineering, vol. 71, no. 2, pp. 197-224, 1988, doi: 10.1016/0045-7825(88)90086-2.

[5] R. D. Matthews, D. Worcester, B. H. Wood, and T. Ryan, "The 1984 Formula SAE Intercollegiate Competition," SAE Technical Paper 841163, 1984, doi: 10.4271/841163.

[6] P. C. Paris and F. Erdogan, "A Critical Analysis of Crack Propagation Laws," Journal of Basic Engineering, vol. 85, no. 4, pp. 528-533, 1963, doi: 10.1115/1.3656900.

[7] B. Patzák and Z. Bittnar, "Design of object oriented finite element code," Advances in Engineering Software, vol. 32, no. 10-11, pp. 759-767, 2001, doi: 10.1016/S0965-9978(00)00090-5.

[8] W. Schütz, "A history of fatigue," Engineering Fracture Mechanics, vol. 54, no. 2, pp. 263-300, 1996, doi: 10.1016/0013-7944(95)00178-6.

[9] K. Svanberg, "The method of moving asymptotes-a new method for structural optimization," International Journal for Numerical Methods in Engineering, vol. 24, no. 2, pp. 359-373, 1987, doi: 10.1002/nme.1620240207.

[10] C. Zillober, "A globally convergent version of the method of moving asymptotes," Structural Optimization, vol. 6, pp. 166-174, 1993, doi: 10.1007/BF01743509.

[11] OptimumG, "OptimumLap - Student Edition," software model description. Available: https://students.optimumg.com/product/optimumlap/ (accessed 9 October 2026).

[12] Yamaha Motor Corporation, U.S.A., YZF-R6R/YZF-R6SR/YZF-R6RC/YZF-R6SRC Service Manual, 1st ed., P/N LIT-11616-16-45, December 2002, p. 2-9.

[13] Donghua Chain, Motorcycle Chains, product catalogue, p. 14, n.d. Available: https://www.dhchain.us/wp-content/files_mf/reduced-motorcyclechains.pdf (accessed 9 October 2026).

[14] K. M. Marshek, "On the analyses of sprocket load distribution," Mechanism and Machine Theory, vol. 14, no. 2, pp. 135-139, 1979, doi: 10.1016/0094-114X(79)90028-4.

[15] C. J. Lodge and S. C. Burgess, "A model of the tension and transmission efficiency of a bush roller chain," Proceedings of the Institution of Mechanical Engineers, Part C: Journal of Mechanical Engineering Science, vol. 216, no. 4, pp. 385-394, 2002, doi: 10.1243/0954406021525179.